Late-Time Target Response Measured with Terahertz Impulse Ranging

R. Alan Cheville, Roger W. McGowan, and Daniel R. Grischkowsky, *Fellow, IEEE*

Abstract— **Time-domain impulse-scattering measurements of freely propagating single cycle terahertz radiation from dielectric targets is measured in the far field with subpicosecond resolution. Initial specular reflection as well as late-time response of the targets is observed to approximately 100 times the initial pulse width. Measured scattered fields agree well with the calculated scattering for early- and late-time response in both the time and frequency domains. The data is fit to both an inverse Fourier transform of numerically calculated frequency domain scattering as well as an intuitive model based on physical optics (PO). The PO picture is verified directly in the time domain and surface wave propagation velocities are measured.**

Index Terms— **Electromagnetic scattering, inverse problems, time-domain measurements.**

I. Introduction

ALTHOUGH there has been a large volume of work published on theoretical calculations of the transient response from various objects [1], the published experimental work on transient scattering is more limited. Early time-domain scattering measurements utilizing electronic pulse-generation techniques with bandwidths of several gigahertz [2] provided much impetus for the theoretical work. Recent time-domain scattering measurements have extended this frequency range using electronic [3], [4] and optoelectronic [5]–[8] pulse-generation methods to measure the impulse response of targets. Electronically generated pulses have demonstrated features as short as 50 ps corresponding to frequency bandwidths extending to 20 GHz [4]. We have previously shown that optoelectronic terahertz impulse ranging can generate pulses with subpicosecond features and frequency bandwidths of over 1 THz [8].

In this paper, we demonstrate the ability of terahertz impulse ranging to determine the response of scale targets by measuring the late time response of dielectric cylinders and spheres. The accuracy of this scale ranging technique is verified by comparing the measured late time response to the numerically calculated response in both the time and frequency domain. We are able to measure the late-time response to many times the initial pulse width, obtaining excellent agreement with the calculated response by frequency-domain scattering calculations combined with Fourier analysis as well as a more intuitive physical optics (PO) model. We have measured the delayed response associated with the creeping wave on the cylinder and have thereby determined that the propagation velocity is c, the velocity of light in free-space. To our knowledge, this is the first direct time-domain confirmation of the applicability of PO approximations for the propagation of creeping waves external to the dielectric cylinder.

Manuscript received May 1, 1996; revised April 9, 1997. This work was supported in part by the National Science Foundation under Grants PHY-9422952 and ECS-9521030 and by the Army Research Office under Grant DAAH04-96-1-0396.

The authors are with the School of Electrical and Computer Engineering and Center for Laser and Photonics Research, Oklahoma State University, Stillwater, OK 74078 USA.

Publisher Item Identifier S 0018-926X(97)07221-9.

II. Experiment

The optoelectronic ranging system (shown in Fig. 1) is a modification of the terahertz beam system [9] used for terahertz time-domain spectroscopy (THz-TDS) [10]. Compared to the previous ranging studies [8], the ranging system shown has been significantly improved by placing a large silicon lens in the transmitted beam and locating the target at the beam waist of the lens. The terahertz ranging pulses are optoelectronically generated by ultrashort laser pulses incident on the optoelectronic source chip. The generated terahertz beam is collimated by a silicon lens, then propagates and diffracts to an off-axis paraboloidal mirror where the terahertz radiation is recollimated into a highly directional beam. This combination of the paraboloidal mirror, silicon lens, and the optoelectronic terahertz source chip comprise the terahertz transmitter; a similar combination comprises the terahertz receiver.

The initial system alignment is performed with the flat deflecting mirrors removed from the terahertz beam (dashed position in Fig. 1). For subsequent measurements the deflecting mirrors are inserted to direct the terahertz beam toward the target. The distances in Fig. 1 are roughly to scale, but the target size has been increased 20 times for clarity. The focal length f of the paraboloidal mirrors is 11.9 cm, the deflecting mirrors are 15 cm from the center of the paraboloidal mirrors, and the target position is 51 cm from the deflecting mirrors, corresponding to 156 cm between the source and receiver chips. The experimental arrangement shown in Fig. 1 at the given target distance of 78 cm (12 + 15 + 51 cm) is bistatic with an angle between source and detector turning mirrors of 11°. The entire system is contained within an enclosure purged with dry air to mitigate absorption by water vapor [11].

The fact that the terahertz beam comes from a point source enables any beam characteristics to be achieved with suitable optics. To a good approximation for the arrangement used

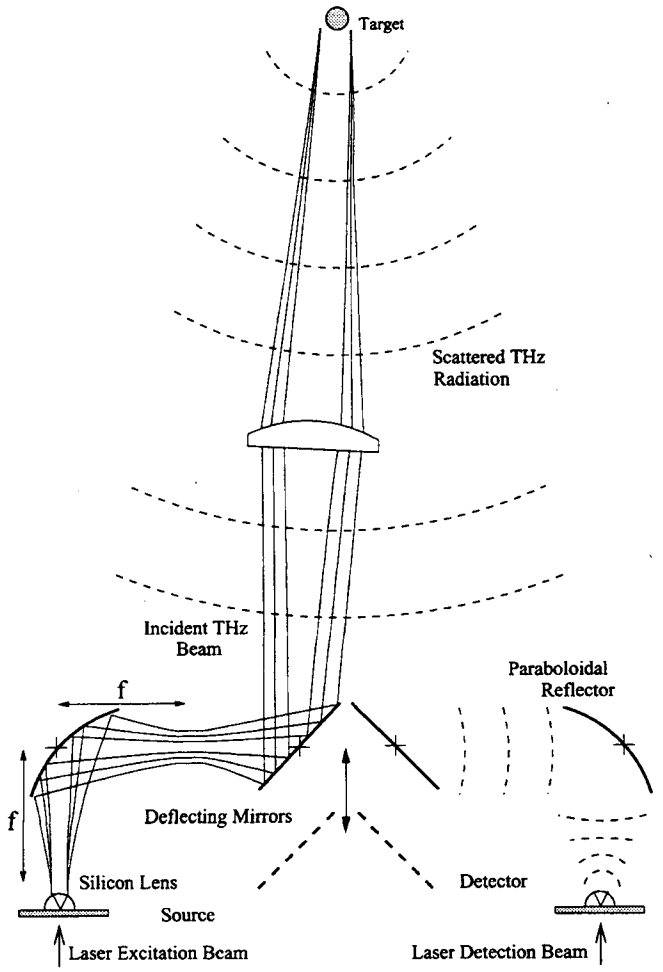

Fig. 1. Terahertz impulse ranging system.

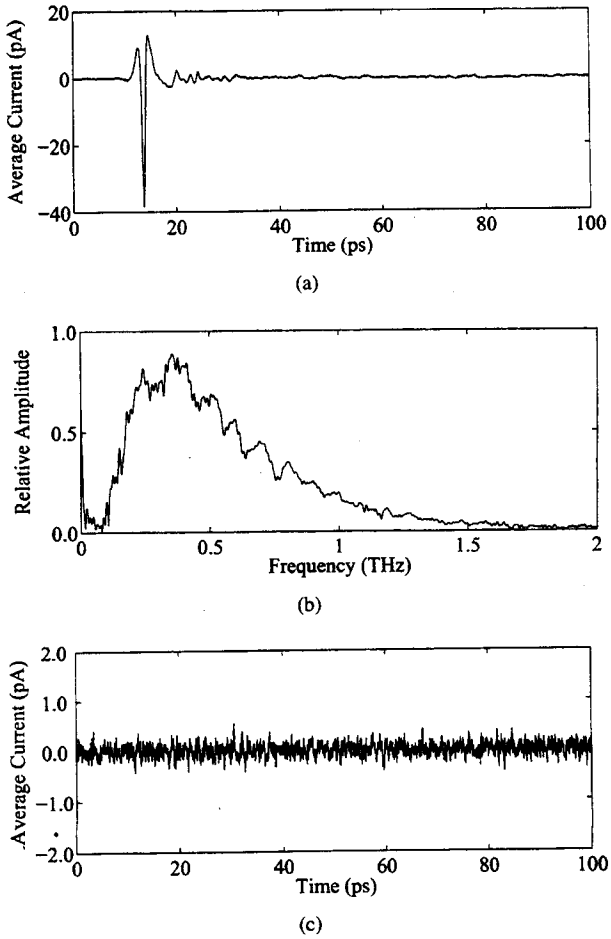

Fig. 2. (a) Spherical wave reference pulse, measured by replacing target with 25.4-mm-diameter metal sphere. (b) Amplitude spectrum of pulse in Fig. 2(a). (c) Returned signal with no target in beam path.

here, the terahertz beam has a Gaussian profile with a 3.8-mm radius waist ($1/e$ point in field) at the face of the silicon lens [12]. The off-axis paraboloidal mirror, located a focal distance $f = 11.9$ cm from the surface of the silicon lens, generates a second waist whose diameter is proportional to wavelength—a distance f beyond the mirror, as shown in Fig. 1. The previously reported ranging system [8] was significantly improved by placing a positive 1-cm-thick 5-cm-diameter high-resistivity [10] silicon lens with a 28-cm focal length in the transmitted beam. The lens was placed in the confocal position, 28 cm from the beam waist produced by the collimating paraboloidal mirror of the transmitter. The target position was moved to be at the focal plane of this lens, i.e., 28 cm from the lens. This arrangement produces a frequency independent 8-mm radius ($1/e$ point in field) beam waist at the target, thereby illuminating the target with a plane wave and eliminating the phase variation across the target.

The spherical wave reference terahertz pulse, measured using a convex spherical metal mirror in place of the target is shown in Fig. 2(a). The observed noise in front of the main pulse is 0.13-pA root mean square (rms) for an integration time of 100 ms. An identical noise value is obtained when the terahertz beam is completely blocked. The amplitude signal-to-noise (S/N) ratio in this single 8.5 min scan consisting of 2048 data channels is greater than 300 : 1. The amplitude spectrum of the incident pulse obtained by a numerical fast Fourier transform (FFT) is shown in Fig. 2(b). The short temporal duration of the pulses results in a bandwidth that extends from approximately 100 GHz to 1.4 THz with a full width at half maximum (FWHM) of 0.5 THz. Fig. 2(c) shows the measured "scattered pulse" with no target in place. No response is seen within the S/N limits of the system, indicating the ability of the fast detector to gate out unwanted reflections.

III. Results

Calibration of the terahertz impulse range was accomplished by measuring the time-domain scattered signature from several dielectric targets. Dielectric targets have a richer structure and a response to much longer times than the conducting targets measured previously [8]. Scattering from a solid dielectric cylinder of fused quartz was measured for electric fields perpendicular to the cylinder axis. Scattering was also measured for an alumina sphere. The real and imaginary components of the index of refraction of fused quartz and alumina have been published previously [10], [13].

We first examine the response of the dielectric cylinder. The measured scattered terahertz pulse from a 3.20 $\pm$0.04-mm-diameter quartz cylinder is shown in Fig. 3(a). The cylinder axis is oriented perpendicular to the incident electric field.

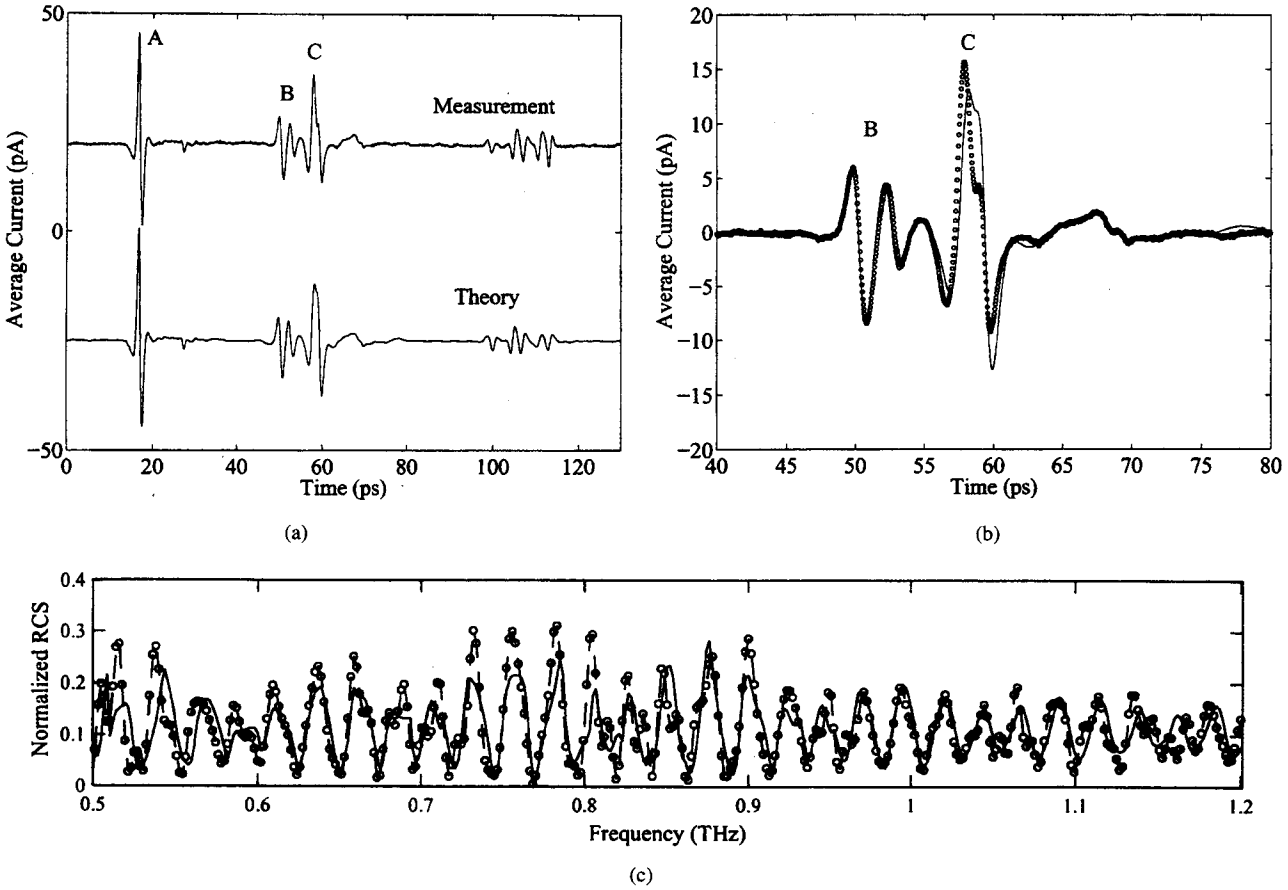

Fig. 3. (a) Measured time-domain reflection (upper curve) compared to calculated reflection (lower curve) from a 3.2-mm-diameter fused quartz cylinder. (b) Comparison of measurements (open circles) and theory (solid line) on an expanded time scale for pulses B and C. (c) Corresponding measured (open circles) and calculated (solid line) normalized radar cross section (RCS). The dashed line is a guide to the eye.

In order to increase the resulting S/N ratio by the square root of the number of scans, the data shown is an average of four individual scans taken consecutively. The amplitude of the scattered specular reflection is larger than that of the spherical wave reference pulse shown in Fig. 2(a). Oscillations in the late-time response can be seen to 100 ps after the initial specular reflection, labeled A in Fig. 3(a).

Our procedure to characterize the frequency-dependent cross section of an actual target is as follows. The pulse incident upon the target as a function of frequency $E_{\rm inc}(\omega)$ can be expressed as the actual generated pulse $P_t(\omega)$ multiplied by a factor $G_t(\omega)$ describing the effects of the source antenna and optics. For the well-collimated beam generated by the terahertz system, the pulse incident upon the target is then $E_{\rm inc}(\omega) = P_t(\omega)G_t(\omega)$. The scattered pulse at the receiver is $E_{\rm sc}(\omega) = E_{\rm inc}(\omega)T(\phi,\omega,r)F_{\rm tr}(\omega)G_r(\omega)$ where $G_r(\omega)$ describes the receiver response and optics and $T(\phi,\omega,r)$ is the scattering function of the target, including propagation effects. $F_{\rm tr}(\omega)$ describes the optical transfer function for the incoming wave from the target with respect to the receiver and is determined by the beam size and wave-front curvature (spherical or cylindrical). The angle ϕ is the bistatic angle and r is the distance from the target to the receiver. The system response is measured by replacing the target with a reference mirror much larger than the beam diameter. This mirror is assumed to be an infinite perfect reflector since even at the longest wavelengths (3 mm, 100 GHz) the reflector used was many wavelengths in extent. In this case, $T(\phi,\omega,r) = 1$ for all frequencies. The signal detected at the receiver from the perfect reflector is then $E_{\rm Ref}(\omega) = P_t(\omega)\ G_t(\omega)F_{\rm mr}(\omega)G_r(\omega)$ where $F_{\rm mr}(\omega)$ describes the optical transfer function for the incoming wave from the mirror with respect to the receiver.

The system response can now be mostly eliminated from the results, leaving only the desired frequency-dependent cross section multiplied by the ratio of the optical transfer functions. For an actual target the signal detected at the receiver is $E_{\rm sc}(\omega) = P_t(\omega)\ G_t(\omega)F_{\rm tr}(\omega)\ G_r(\omega)T(\phi,\omega,r)$. By taking the ratio of the amplitude spectra of the scattered response from the target and the reference reflector, the effects of antennas and optics are removed from the data, and we obtain the measured scattering function multiplied by the ratio of the optical transfer functions $E_{\rm sc}(\omega)/E_{\rm Ref}(\omega) = T_{\rm meas}(\phi,\omega,r)F_{\rm tr}\ (\omega)/F_{\rm mr}(\omega)$ where distant dependent propagation terms are included in $T_{\rm meas}(\phi,\omega,r)$. In the far-field limit for which the incident waves to the receiver can be treated as plane waves, the optical transfer functions for the target and mirror are then the same and $E_{\rm sc}(\omega)/E_{\rm Ref}(\omega) = T_{\rm meas}(\phi,\omega,r)$. Alternatively, if the mirror used to measure the reference pulse has the same geometry and thus produces the same wavefront curvature at the receiver as for the target, the ratio $F_{\rm tr}(\omega)/F_{\rm mr}(\omega)$ is unity. For a known distance

r from the target to the detector the measured scattering parameter, $T_{\text{meas}}(\phi, \omega)$ can then be compared to that calculated numerically in the frequency domain $T_{\text{calc}}(\phi, \omega)$.

These measurements permit direct determination of the frequency and aspect dependent radar cross section (RCS). For a given distance r from the target, the normalized RCS for a cylindrical $(n = 1)$ and spherical $(n = 2)$ target is

$$\sigma_{\text{RCS}} = \frac{4\pi^n}{\pi k_0^n}|T(\omega, \varphi)|^2 \frac{1}{\pi a^n} = \pi(2r)^n \left|\frac{E_{\text{sc}}}{E_{\text{Ref}}}\right|^2 \frac{1}{\pi a^n} \quad (1)$$

where $T(\omega, \phi)$ is the scattering function, E_{Ref} and E_{sc} are the reference and scattered electric fields, respectively, a is the target radius, r is the target-detector distance, and $k_0 = 2\pi/\lambda_0$ is the wavevector in free-space, and the distance dependence is now given separately from $T(\omega, \phi)$. The scattered electric field E_{sc} is determined as a function of frequency from the numerical Fourier transform of the time domain data. For the quartz cylinder, E_{sc} is shown in Fig. 3(a) and (b). The reference electric field E_{Ref} is determined from a reference pulse, similar to that shown in Fig. 2, except that a cylindrical mirror was used. The measured normalized RCS is shown as open circles in Fig. 3(c).

Given the complex index of refraction of fused quartz, the frequency dependent RCS of the solid dielectric cylinder may be calculated exactly. The scattered electric field is given by the relationship [14], [15]

$$E_{\text{sc}}(\omega, r) = E_{\text{inc}}(\omega)\sqrt{\frac{2}{\pi k_o r}} e^{i(k_o r - \pi/4)} T(\omega, \phi) \quad (2)$$

where $E_{\text{inc}}(\omega) = P_t(\omega)G_t(\omega)$ is the incident electric field, r is the distance from the scatterer to the detector, and $T(\omega, \phi)$ depends upon the target composition, polarization of the incident wave relative to the target orientation, and the bistatic angle ϕ between the incident and scattered wave. For a dielectric cylinder the T terms may be calculated numerically as outlined in [15]. Such calculations of the scattering coefficients were performed in MatLab running on an IBM PC with a 486 processor or a Sun SPARC 20 for large data sets. The calculated RCS with the summation taken to $n = 80$ is shown as the solid line in Fig. 3(c). Agreement is good from 0.5 to 1.2 THz. The quality of the measured scattered data degrades beyond 1.2 THz. The amplitude of the frequency components of the incident pulse beyond 1.2 THz is reduced by at least a factor of five with respect to those at the peak, reducing the measurement sensitivity at the higher frequencies.

The response of the dielectric cylinder to the incident terahertz pulse may also be calculated in the time domain given the cylindrical wave reference pulse shape and the calculated complex scattering coefficient. This is done by multiplying the complex, frequency dependent scattering coefficient with the amplitude and phase components of the reference pulse (measured by replacing the target with a cylindrical reference mirror) and numerically converting to the time domain by an inverse Fourier transform [5], [8], [15]. The calculated scattered field for the 3.2-mm diameter dielectric cylinder is shown in Fig. 3(a). Measurement and calculations agree quite well for echoes occuring more than 100 ps following the initial specular reflection. This corresponds to a temporal window of over 100 times the initial pulse width and validates the accuracy of the terahertz impulse range for both the initial transient as well as the late-time response. Similar agreement is obtained over a range of target sizes from $k_c a = 8.8$ to 26.8, where k_c is the wave vector in free-space at the peak of the reference pulse spectrum. Across the reference pulse spectrum, $k_o a$ varies from 2.1 for the smallest targets at 100 GHz to 76.7 for the largest targets at 1.2 THz.

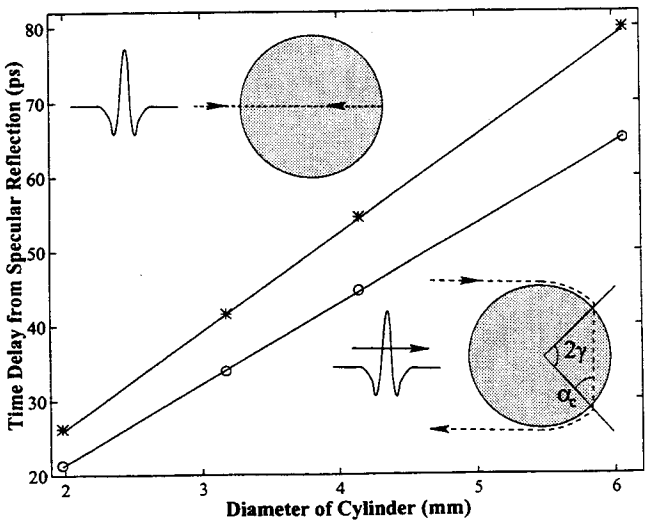

Fig. 4. Measured delay between specular reflection and back axial (stars) and surface waves (open circles) as a function of cylinder diameter. The lines are predicted values from the PO picture. The insets show the B and C reflections.

In contrast to the complicated frequency-domain results, the simple structure of the time-domain response is open to analysis by a more intuitive model based on PO [16]–[18], by determining the time delay between features in the delayed response-pulse train. The salient features of this model are extrapolated from a spherical to our cylindrical geometry. The accuracy of this PO model is strongly dependent upon the ability to measure well-resolved scattered pulses directly in the time domain. As shown in Fig. 3(b), we are able to measure peaks separated by 7 ps with temporal resolution under 500 fs. We concentrate on the first two reflected pulses labeled B and C in Fig. 3(a) and (b) following the initial specular reflection A. The second reflection at 58.1 ps, C is due to a pulse that makes a single round trip through the cylinder, as shown in the top inset to Fig. 4. The expected delay $\Delta\tau_C$ between the specular front-surface reflection and the back-surface reflection from a simple PO picture is $\Delta\tau_C = 4an/c$. The cylinder radius is a and the real part of the index of refraction is $n \cong 1.952$ for fused quartz [10]. For our case, the calculated value is 41.6 ± 0.5 ps compared to the measured value of 40.9 ps. The B pulse at 50.9 ps is inverted with respect to C and is due to a portion of the incident field that strikes the cylinder at grazing incidence and begins to propagate around the circumference as a surface wave [16]–[18]. This surface wave can take one or more detours through the cylinder, entering at the critical angle α_c and exiting again to travel as a surface wave. The case of a single traverse around the cylinder circumference with one detour corresponds to the B pulse shown in the lower inset to

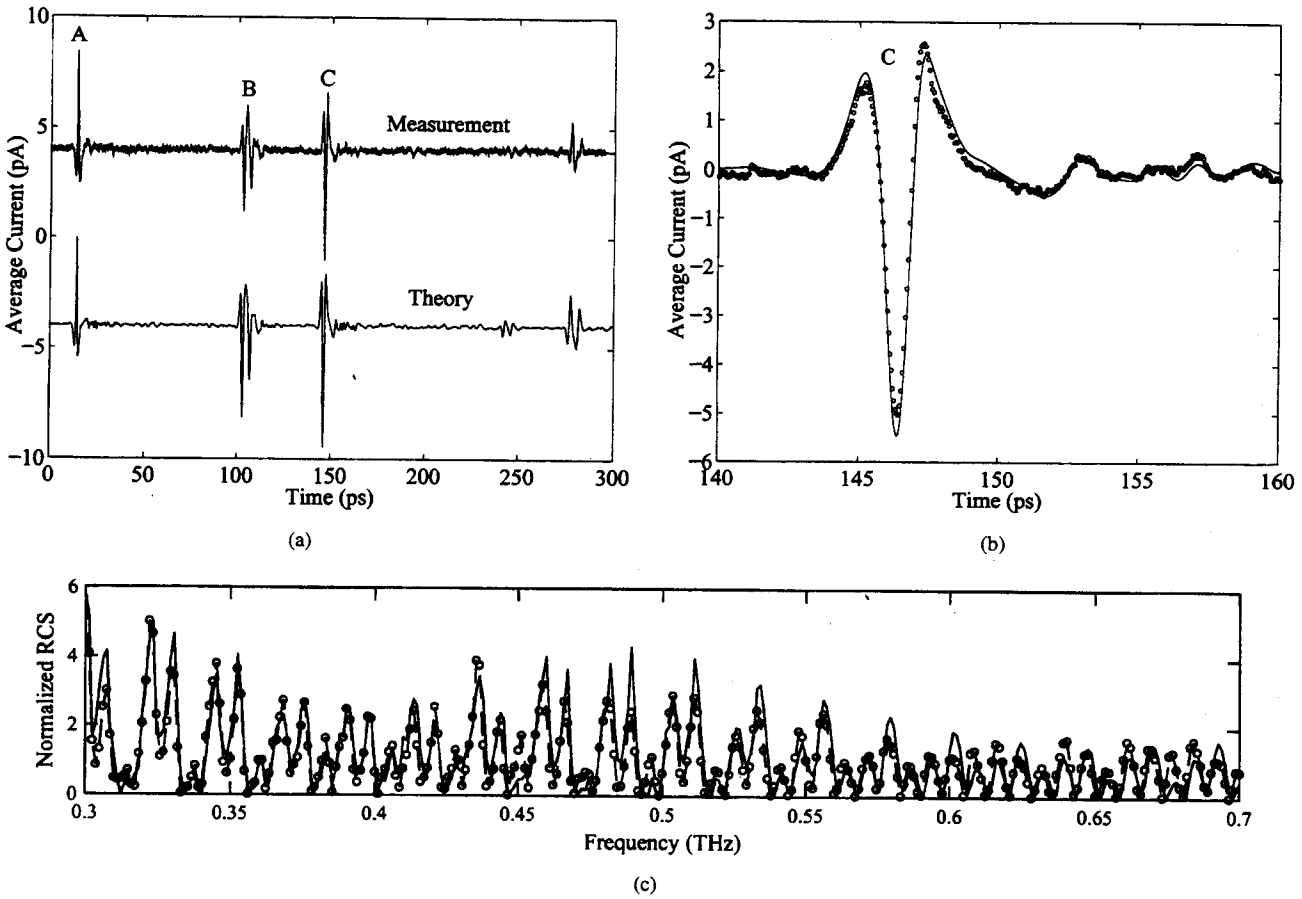

Fig. 5. (a) Measured time-domain reflection (upper curve) compared to calculated reflection (lower curve) from a 6.35-mm-diameter alumina sphere. (b) Comparison of measurements (open circles) and theory (solid line) on an expanded time scale for pulse C. (c) Corresponding measured (open circles) and calculated (solid line) normalized RCS. The dashed line is a guide to the eye.

Fig. 4. This pulse is delayed from the specular reflection by $\Delta\tau_B = [2a + an_{\text{eff}}(\pi - 2\gamma)]/c + \kappa$ where κ is the additional time for the pulse to "detour" through the cylinder rather than travel as a surface wave and is given by $\kappa = [2na\sin\gamma]/c$ where γ is determined by the critical angle $\alpha_c = \arcsin(1/n)$ with $\gamma = \pi/2 - \alpha_c$. The surface wave travels at a velocity c/n_{eff} with n_{eff} an "effective refractive index." The details of this model have been examined by several authors for spherical geometry with disagreement on the value of n_{eff} [16]–[18].

The two different physical paths that correspond to the axial and first surface wave returns are illustrated by measuring the peak of the reflected pulses B and C with respect to the peak of the specular reflection A for various fused quartz cylinder diameters. The measured delay between the specular A pulse and those of pulse B that travels the cylinder circumference (open circles) and the pulse C that makes one round trip through the cylinder (stars) is shown as a function of cylinder diameter in Fig. 4. The solid lines are calculated values of $\Delta\tau_B$ and $\Delta\tau_C$ with $n = 1.952$ and $n_{\text{eff}} = 1$. The straight line fit to the position of the returned surface pulse B is within our experimental error for $0.95 < n_{\text{eff}} < 1.12$. This measurement shows the surface waves propagate on the cylinder with a group velocity near that of free-space. For these same diameters we have calculated, by inverse Fourier transform of the frequency domain scattering, the delay of pulses A, B, and C. From the time separation of these pulses, we obtain a group velocity of c for the surface wave. This result is in agreement with our experiment as well as [16] and [18], which considered the sphere. To our knowledge, this is the first direct time-domain confirmation of the applicability of the PO approximation for the propagation of creeping waves external to a dielectric cylinder. These results also illustrate how the high-temporal resolution of terahertz time domain ranging can elucidate the physical mechanisms of scattering processes.

The later pulses at approximately 110 ps can also be assigned to a geometrical optics model. Although our S/N ratio is not sufficient to fully resolve all the features, these pulses are due to two contributions. The first contribution is a stationary ray [15] which has traversed the cylinder five times undergoing four internal reflections. The second contribution is from surface waves (same as pulse B) making a total of 3π rotations around the cylinder with four detours through the cylinder.

The scattered radiation from an alumina sphere 6.35 mm in diameter is shown in Fig. 5. The sphere was supported on a Styrofoam pedestal shaped to reflect the incident radiation away from the detector. No signal was detected from the pedestal without the sphere present, due to the low refractive

index of Styrofoam in the terahertz region. The response of the sphere is considerably smaller than that of the cylinder due to the $1/r^2$ dependence of radiation scattered from a spherical target opposed to the $1/r$-power dependence of that from a cylinder; the cross-sectional area of the sphere seen by the incident terahertz beam is approximately 0.75 that of the solid cylinder. The data shown is an average of eight individual scans. Also shown in Fig. 5(a) as the lower curve is the calculated response of a homogeneous dielectric sphere of $n = 3.12$ for a synthesized pulse shape matching that of Fig. 2(a). The excellent agreement between theory and experiment shown in Fig. 5(a) confirms both the accuracy of the experimental system and the theoretical approach. This high precision is also highlighted in the data overlay of Fig. 5(b).

The temporal pulses shown in Fig. 5(a) are characterized similar to the cylindrical case. Pulse A is the specular reflection from the surface of the sphere. Pulse B is due to a surface wave, and pulse C is the axial reflection from the back surface of the sphere. Pulse C arrives $\Delta t_c = 4an/c = 132.3$ ps after the specular reflection A. This yields an effective index of refraction of $n = 3.12$, which is used in the calculation. The time separation between these well-resolved calculated pulses shows that for the spherical case as well, the surface wave propagates with a group velocity near c.

Again, given the complex index of refraction of the alumina sphere [13], the frequency-dependent RCS of the sphere may be calculated exactly [14], [15] and is shown as the solid line in Fig. 5(c). Here, the agreement between the measurements and theory is quite precise and demonstrates the accuracy of terahertz impulse ranging over a broad frequency range.

IV. Conclusion

We have demonstrated the ability of terahertz impulse ranging systems to measure the late-time response of dielectric targets following excitation by a short impulse-like pulse. Measurements with the terahertz system have shown excellent agreement with theoretically predicted returns from several targets both in the time and frequency domain. Results agreed well with an intuitive model based on PO, which permitted measurement of surface wave velocities.

To assess the suitability of terahertz impulse ranging for characterizing real-world targets using geometrically scaled models, work will be needed to identify dielectrics with similar permittivity over a wide-frequency range. The signature from highly conductive metal targets is predicted to be accurate in this frequency range [19].

Further extension of this work beyond the simple targets and model aircraft measured so far has many possibilities. Experimental verification of predicted scattering from more complex objects of interest has been mentioned previously. The ability to construct small-scale dioramas would permit the investigation of target detection in ground or sea clutter. Such models could also be used to test techniques for locating underground or hidden targets provided the dielectric properties of soil in the frequency range of interest could be reproduced.

References

[1] D. A. Vechinsky, S. M Rao, and T. K. Sarkar, "Transient scattering from three-dimensional arbitrarily shaped dielectric bodies," *J. Opt. Soc. Amer. A*, vol. 11, pp. 1458–1470, 1994.

[2] E. K. Miller and J. A. Landt, "Direct time-domain techniques for transient radiation and scattering from wires," *Proc. IEEE*, vol. 68, pp. 1396–1423, Nov. 1980.

[3] H. C. Strifors, G. C. Gaunnard, B. Brusmark, and S. Abrahamson, "Transient interactions of an EM pulse with an dielectric spherical shell," *IEEE Trans. Antennas Propagat.*, vol. 42, pp. 453–462, Apr. 1994.

[4] M. Morgan, "Ultrawideband impulse scattering measurements," *IEEE Trans. Antennas Propagat.*, vol. 42, pp. 840–846, June 1994.

[5] L. Carin, in *Ultra-Wideband, Short-Pulse Electromagnetics*, H. Bertoni, Ed. New York: Plenum, 1993, pp. 37–49.

[6] W. M. Robertson, G. V. Kopcsay, and G. Arjavalingam, "Picosecond time-domain electromagnetic scattering from conducting cylinders," *IEEE Microwave Guided Wave Lett.*, vol. 1, pp. 379–381, Dec. 1991.

[7] A. Rahman, D. Kralj, L. Carin, M. R. Melloch, and J. M. Woodall, "Photoconductively switched antennas for measuring target resonances," *Appl. Phys. Lett.*, vol. 64, pp. 2178–2180, 1994.

[8] R. A. Cheville and D. Grischkowsky, "Time domain THz impulse ranging studies," *Appl. Phys. Lett.*, vol. 67, pp. 1960–1962, 1995.

[9] M. van Exter and D. Grischkowsky, "Characterization of an optoelectronic TeraHz beam system," *IEEE Trans. Microwave Theory Tech.*, vol. 38, pp. 1684–1691, Nov. 1990.

[10] D. Grischkowsky, S. Keiding, M. van Exter, and Ch. Fattinger, "Far-infrared time-domain spectroscopy with terahertz beams of dielectrics and semiconductors," *J. Opt. Soc. Amer. B*, vol. 7, pp. 2006–2015, 1990.

[11] M. van Exter, Ch. Fattinger, and D. Grischkowsky, "Terahertz time-domain spectroscopy of water vapor," *Opt. Lett.*, vol. 14, pp. 1128–1130, 1989.

[12] P. Uhd Jepsen and S. R. Keiding, "Radiation patterns from lens-coupled terahertz antennas," *Opt. Lett.*, vol. 20, pp. 807–809, 1995.

[13] M. N. Afsar and K. J. Button, "Millimeter-wave dielectric properties of materials," in *Infrared and Millimeter Waves*. New York: Academic, 1984, vol. 12.

[14] R. F. Harrington, *Time Harmonic Electromagnetic Fields*. New York: McGraw-Hill, 1961.

[15] D. E. Barrick, *Radar Cross Section Handbook*, G. T. Ruck, Ed. New York: Plenum, 1970, vol. 1.

[16] J. Rheinstein, "Backscatter from spheres: A short pulse view," *IEEE Trans. Antennas Propagat.*, vol. AP-16, pp. 89–97, Jan. 1968.

[17] H. Inada, "Backscattered short pulse response of surface waves from dielectric spheres," *Appl Opt.*, vol. 13, pp. 1928–1933, 1974.

[18] M. S. Aly and T. T. Y. Wong, "Scattering of a transient electromagnetic wave by a dielectric sphere," *Proc. Inst. Elect. Eng.*, vol. 138, pt. H, pp. 192–198, Apr. 1991.

[19] C. R. Schumacher, "Electrodynamic similitude and physical scale modeling of nondispersive targets," *J. Appl. Phys.*, vol. 67, pp. 2616–2625, 1987.

R. Alan Cheville received the B.S.E.E. and Ph.D. degrees from Rice University, Houston, Texas, in 1986 and 1994, respectively.

Currently, he is a Visiting Assistant Professor in the Department of Electrical and Computer Engineering at Oklahoma State University, Stillwater, OK. His current research interests are focused on applications of optoelectronically generated terahertz radiation including spectroscopy of molecular vapors, far-infrared characterization of combustion, and terahertz impulse ranging. Formerly, he was involved in electron beam-pumped tunable excimer lasers, broadly tunable second-harmonic generation systems for short-pulse lasers, and ultrafast time-resolved spectroscopy of semiconductors and fullerene films.

Dr. Cheville is a member of the APS Laser Science Division and the Optical Society of America.

Roger W. McGowan was born in St. Paul, MN, on July 7, 1966. He received the B.A. degree in physics from Gustavus Adolphus College, St. Peter, MN, in 1988, and the Ph.D. degree in physics from Colorado State University, Fort Collins, CO, in 1996.

In May 1996, he accepted a Post Doctoral Fellowship at Oklahoma State University, Stillwater, OK, where he is currently working in the multidisciplinary Center for Laser and Photonic Research. His research interests include ultrafast optoelectronics, generation and applications of terahertz radiation, and ultrashort electrical pulse propagation on microtransmission lines.

Dr. McGowan is a member of the Optical Society of America and the American Physical Society.

Daniel R. Grischkowsky (A'84–SM'90–F'92) was born in St. Helens, OR, on April 17, 1940. He received the B.S. degree from Oregon State University, Corvallis, OR, in 1962 and the Ph.D. degree in physics from Columbia University, New York, NY, in 1968.

In 1969, he joined IBM at the Watson Research Center, Yorktown Heights, NY. His initial experimental and theoretical research involved studying the interaction between near-resonant light and the two-level system. His studies of the nonlinear propagation of picosecond laser pulses in single-mode optical fibers led to the invention of the optical-fiber pulse compressor and to the experimental observations of gray solitons and optical intensity shocks. Currently, his work involves ultrafast optoelectronics, initially focusing on the generation and applications of subpicosecond electrical pulses on transmission lines. In 1993 he joined Oklahoma State University, Stillwater, as the Bellmon Professor of Optoelectronics in the School of Electrical and Computer Engineering.

Dr. Grischkowsky is a Fellow of the Optical Society of America and the American Physical Society. He was awarded the Boris Pregel Award for Applied Science and Technology in 1985 by the New York Academy of Sciences for his invention of the optical fiber pulse compressor. He also received the R.W. Wood Prize in 1989 from the Optical Society of America for his pulse propagation studies in optical fibers and their use for generating ultrashort pulses of light.